176

Robots and Controls

Thomas R. Kurfess
Georgia Institute of Technology

Mark L. Nagurka
Marquette University

Credit for bringing robots to life is given to two individuals, Karel Capek and Isaac Asimov. In 1922, Capek wrote a play called *Rossum's Universal Robots* (RUR) describing how robots would turn on mankind and eventually take over the world. In the 1940s, Asimov, who is credited with coining the term "robotics," freed us from a view of robots as malevolent beings, painting a view of robots as our helpmates, improving our lives and making us more productive.

176.1 Robot Definition

The term "robot" is defined by The Robotics Industry Association as a "reprogrammable multifunctional manipulator designed to move material, parts, tools, or specialized devices, through variable programmed motions for the performance of a variety of tasks." It consists of mechanical links, often in a serial chain with one link grounded or attached to a frame, that are connected via revolute (i.e., hinge) or prismatic (i.e., sliding) joints and actuated via gear trains or directly by electric motors or hydraulic or pneumatic drives. A robot will generally include position sensors (such as potentiometers or optical encoders) and may include contact, tactile, force/torque, proximity, or vision sensors. At its distal end, a robotic manipulator is typically fitted with an end-effector, such as a gripper, enabling it to accomplish desired tasks. An example of an industrial robot is the Case Packer from CAMotion, Inc. shown in Figure 176.1.

176.2 Robot Control Problem

The fundamental control problem in robotics is to determine the actuator signals required to achieve the desired motion and specified performance criteria. If the robot is to perform a task while in contact with a surface, it is also necessary to control the contact force applied by the manipulator. Although the control problem can be stated simply, its solution may be quite complicated due to robot nonlinearities. For example, because of coupling among links, the robot dynamics in a serial link robot design are described mathematically by a set of coupled nonlinear differential equations, making the controls problem challenging. The controls problem becomes even more difficult if the links exhibit flexibility, and hence cannot be modeled as rigid.

0-8493-1586-7/05/$0.00+$1.50

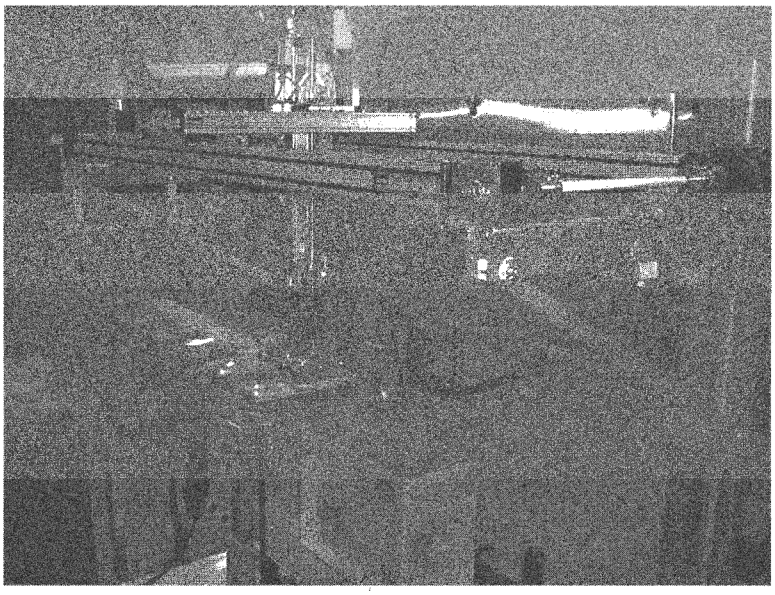

FIGURE 176.1 Case Packer Cartesian Robot. (Courtesy of CAMotion, Inc.)

To achieve the desired motion and possibly contact force characteristics, the planning of the manipulator trajectory is integrally linked to the control problem. The position of the robot can be described by a set of joint coordinates in *joint space* or by the position and orientation of the end-effector using coordinates along orthogonal axes in *Cartesian or task space*. The two representations are related, that is, the Cartesian position and orientation can be computed from the joint positions via a mapping (or function) known as *forward kinematics*. The motion required to realize the desired task is generally specified in Cartesian space. The joint positions required to achieve the desired end-effector position and orientation can be found by a mapping known as the *inverse kinematics*. This inverse kinematics problem may have more than one solution, and a closed-form solution may not be possible, depending on the geometric configuration of the robot. The desired motion may be specified as point to point, in which the end-effector moves from one point to another without regard to the path, or it may be specified as a continuous path, in which the end-effector follows a desired path between the points. A trajectory planner generally interpolates the desired path and generates a sequence of set points for the controller. The interpolation may be done in joint or Cartesian space.

Some of the robot control schemes in use today include independent joint control [Luh, 1983]; Cartesian-space control [Luh et al., 1980]; and force control strategies such as hybrid position/force control [Raibert and Craig, 1981] and impedance control [Hogan, 1985]. In independent joint control, each joint is considered as a separate system and the coupling effects between the links are treated as disturbances to be rejected by the controller. Performance can be enhanced by compensating for robot nonlinearities and interlink coupling using the method of computed torque or inverse dynamics. In Cartesian-space control, the error signals are computed in Cartesian space and the inverse kinematics problem need not be solved. In this chapter, independent joint control is analyzed in depth to provide insight into the use of various controllers for joint position control. Information on force control schemes can be found in the references cited above as well in Bonitz [1995].

176.3 Basic Joint Position Dynamic Model

Many industrial robots operate at slow speeds, employing large gear reductions that significantly reduce the coupling effects between the links. For slowly varying command inputs, the drive system dominates

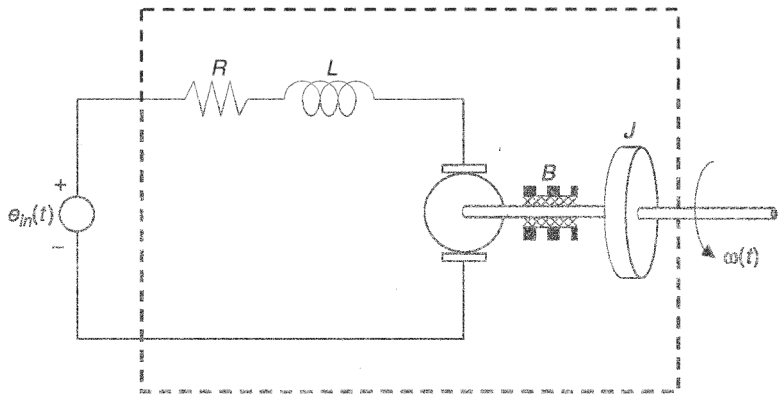

FIGURE 176.2 Simple actuator model for a single-link robot.

the dynamics of each joint and each link can be considered rigid. Under these conditions, each joint can be controlled as an independent system using linear system control techniques. Figure 176.2 is a model of a single actuator-link model, representative of a single link robot. The model includes an effective inertia, J,

$$J = J_m + r^2 J_l \tag{176.1}$$

where r is the gear ratio of the joint, J_m is the motor inertia, and J_l is the link inertia. The model also includes an effective damping coefficient, B, and a motor armature inductance and resistance, L and R, respectively. The relationship between the motor input voltage and the rotational speed is given by the second-order differential equation,

$$\ddot{\omega}(t) + (JR + BL)\dot{\omega}(t) + \left(\frac{RB}{JL} + \frac{K_t^2}{JL}\right)\omega(t) = \frac{K_t}{JL} e_{in}(t) \tag{176.2}$$

where $e_{in}(t)$ is the motor input voltage, $\omega(t)$ is the link angular velocity or rotational speed, and K_t is a motor torque constant (torque per current ratio). Assuming zero initial conditions and defining the Laplace transformations,

$$\Im\{\omega(t)\} \equiv \Omega(s) \qquad \Im\{e_{in}(t)\} \equiv E_{in}(s)$$

the transfer function between the input voltage, $E_{in}(s)$ and the link rotational velocity, $\Omega(s)$, can be written as

$$\frac{\Omega(s)}{E_{in}(s)} = \frac{\dfrac{K_t}{JL}}{s^2 + (JR + BL)s + \left(\dfrac{RB}{JL} + \dfrac{K_t^2}{JL}\right)} \tag{176.3}$$

For most motor systems, the overall system dynamics are dominated by the mechanical dynamics rather than the electrical "dynamics," that is, the effect of L is small in comparison to the other system parameters. Assuming negligible L in equation (176.3), the following first-order transfer function can be developed:

$$\lim_{L\to 0}\left[\frac{\Omega(s)}{E_{in}(s)}\right]=\lim_{L\to 0}\left[\frac{\dfrac{K_t}{JL}}{s^2+(JR+BL)s+\left(\dfrac{RB}{JL}+\dfrac{K_t^2}{JL}\right)}\right]=\frac{K_t}{JRs+\left(RB+\dfrac{K_t^2}{JL}\right)} \tag{176.4}$$

Defining the open-loop joint time constant, T_m, as

$$T_m=\frac{JR}{RB+\left(\dfrac{K_t^2}{JL}\right)} \tag{176.5}$$

and the open-loop link gain as

$$K_m\equiv\frac{K_t}{RB+\left(\dfrac{K_t^2}{JL}\right)} \tag{176.6}$$

Equation (176.4) can be rewritten as

$$\frac{\Omega(s)}{E_{in}(s)}=\frac{K_m}{T_m s+1} \tag{176.7}$$

The assumption of the motor inductance being small, resulting in negligible electrical dynamics is considered reasonable if the negative real part of the single pole from the electrical dynamics is approximately three times larger than the negative real part of the mechanical dynamics. This is known as the dominant pole theory, and is valid for most motors. However, for small motors, such as those used in micro-electromechanical systems (MEMS) devices, this assumption may not be valid.

Equation (176.7) provides a relationship between joint angular velocity and input motor voltage, and is a useful first-order model for velocity control. However, for most robot applications, position control rather than velocity control is desired. For the typical case of lower velocities, the dynamics of the individual joints can be considered to be decoupled. Recognizing that the position of the joint is the integral of the joint velocity, a transfer function between position, $\Theta(s)$, which is the Laplace transform of $\theta(t)$, and the input voltage can be developed:

$$G(s)=\frac{\Theta(s)}{E_{in}(s)}=\frac{\dfrac{1}{s}\Omega(s)}{E_{in}(s)}=\left(\frac{1}{s}\right)\frac{K_m}{T_m s+1}=\frac{K_m}{s(T_m s+1)} \tag{178.8}$$

where $G(s)$ is the plant transfer function for the single link. Equation (176.8) is a model for position control, and the same simple dynamics can be used to model a variety of systems including high precision machine tools, which are essentially multiaxis Cartesian robots [Kurfess and Jenkins, 2000].

176.4 Independent Joint Position Control

For many applications, the assumption of negligible link coupling is reasonable and independent joint position control can be a successful strategy. Two classical control methods — proportional derivative (PD) control and proportional integral derivative (PID) control — are typically implemented. This

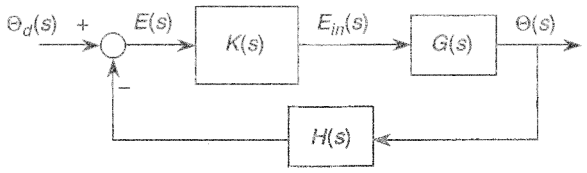

FIGURE 176.3 Generalized closed-loop system configuration.

section develops design strategies for both types, and, for completeness, considers the even simpler proportional (P) controller. Figure 176.3 represents the closed-loop feedback configuration for the single link model, where $G(s)$ represents the link or plant dynamics given by Equation (176.8), $K(s)$ represents the controller that is to be designed, and $H(s)$ represents the feedback sensor dynamics. In general, the relationship between the desired angular position, $\Theta_d(s)$, and the actual angular position of the link, $\Theta(s)$, is given by Black's Law (1934a, 1934b),

$$G_{CL}(s) = \frac{\Theta(s)}{\Theta_d(s)} = \frac{K(s)G(s)}{1 + K(s)G(s)H(s)} \tag{176.9}$$

The angular error, $E(s)$, is given by the difference between the desired angle and the actual angle. The transfer function between $\Theta_d(s)$ and $E(s)$ is given by

$$\frac{E(s)}{\Theta_d(s)} = \frac{\Theta_d(s) - \Theta(s)}{\Theta_d(s)} = \frac{1}{1 + K(s)G(s)H(s)} \tag{176.10}$$

The controller typically includes a power amplifier that provides the power to drive the system. In this example, the output of the controller is a voltage, that is, the power amplifier's function is to provide sufficient current at the desired voltage to drive the system. Saturation occurs when the desired input voltage exceeds the maximum amplifier voltage output capacity, or when the product of the voltage and current exceeds the amplifier's rated power capacity. The effect of saturation is ignored in the following examples. Finally, the controller output voltage can be related to the input command signal via the following transfer function,

$$\frac{E_{in}(s)}{\Theta_d(s)} = \frac{E(s)}{\Theta_d(s)}K(s) = \frac{\Theta_d(s) - \Theta(s)}{\Theta_d(s)}K(s) = \frac{K(s)}{1 + K(s)G(s)H(s)} \tag{176.11}$$

Equation (176.11) can be used to determine the motor command voltage as a function of the desired angular trajectory.

Definition of Specifications

Specifications are generally provided to ensure that the desired system behavior is achieved. The specifications define the closed-loop system characteristics, and the usual practice is to tune the controller gains to achieve the desired performance. For this exercise, a 2% settling time, t_s, and a maximum percent overshoot, M_P, are specified. These two quantities (and others) are visualized in the typical second-order response shown in Figure 176.4. They define a desired dynamic response of the closed-loop system described by a second-order model of the form,

$$G_{CL}(s) = \frac{\omega_{nd}^2}{s^2 + 2\zeta_d\omega_{nd}s + \omega_{nd}^2} \tag{176.12}$$

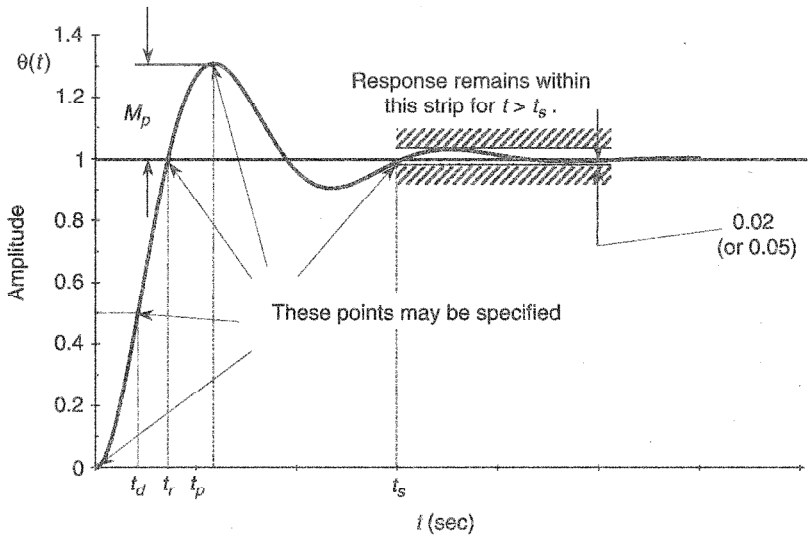

FIGURE 176.4 A typical second-order response.

where ζ_d and ω_{nd} are the desired damping ratio and (undamped) natural frequency, respectively, and are related to the desired overshoot M_{Pd} and desired settling time t_{sd}, of the target closed-loop system by the expressions,

$$M_{Pd} = e^{-\left(\zeta_d/\sqrt{1-\zeta_d^2}\right)\pi} \tag{176.13}$$

$$t_{sd} \approx \frac{4}{\zeta_d \omega_{nd}} \tag{176.14}$$

where the latter is a conservative approximation of the settling time. Solving for ζ_d in Equation (176.13) yields

$$\zeta_d = \sqrt{\frac{\ln(2M_{Pd})}{\pi^2 + \ln(2M_{Pd})}} = \frac{\ln(M_{Pd})}{\sqrt{\pi^2 + \ln(2M_{Pd})}} \tag{176.15}$$

From Equations (176.14) and (176.15), ω_{nd} can be expressed as

$$\omega_{nd} \approx \frac{4\sqrt{\pi^2 + \ln(2M_P)}}{t_{sd}\ln(M_P)} \tag{176.16}$$

From Equation (176.12), the characteristic equation that defines the system response is given by

$$s^2 + 2\zeta_d \omega_{nd} s + \omega_{nd}^2 = 0 \tag{176.17}$$

This equation can be used for the design of various controllers. The poles of the closed-loop system are shown in Figure 176.5 for a variety of desired damping ratios, ζ_d. Nominally, for joint position control a damping ratio of 1, corresponding to a critically damped system, is desired. This places both poles in

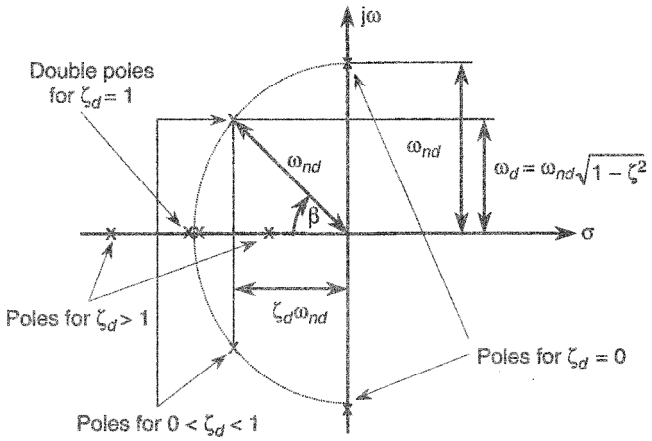

FIGURE 176.5 Pole locations for desired closed-loop system dynamics.

the same location on the real axis, and yields the fastest system response without overshoot. For generality in the control design examples, the variables ζ_d and ω_{nd} are used rather than specific values for these variables [Nagurka and Kurfess, 1992].

Proportional (P) Control

In P control, the simplest analog control algorithm, the control signal is proportionally related to the error signal by a constant gain, K_P. Thus, the transfer function for a proportional controller is a constant,

$$K(s) = K_P \tag{176.18}$$

The closed-loop transfer function of the single actuator-link system with a proportional controller is

$$G_{CL}(s) = \frac{K_P K_m / T_m}{s^2 + (1/T_m)s + K_P K_m / T_m} \tag{176.19}$$

from Equations (176.8), (176.9), and (176.18). The characteristic equation for the transfer function given in Equation (176.19) is

$$s^2 + (1/T_m)s + K_P K_m / T_m = 0 \tag{176.20}$$

With one free design parameter, the proportional gain, K_P, the target closed-loop system dynamics will be virtually impossible to achieve. By equating the actual closed-loop characteristic Equation (176.20) to the desired closed-loop characteristic Equation (176.17),

$$s^2 + (1/T_m)s + K_P K_m / T_m = 0 = s^2 + 2\zeta_d \omega_{nd} s + \omega_{nd}^2 \tag{176.21}$$

only ω_{nd} can be specified directly, giving the value of K_P by

$$K_P = \omega_{nd}^2 \frac{T_m}{K_m} \tag{176.22}$$

(found by equating the coefficients of s^0). Once ω_{nd} has been chosen, ζ_d is fixed to be

$$\zeta_d = \frac{1}{2\omega_{nd} T_m} \tag{176.23}$$

It is useful to investigate the location of the closed-loop poles as a function of K_P. The pole locations on the s-plane can be computed by solving for s in Equation (176.21) via the quadratic formula,

$$s = \frac{-\frac{1}{T_m} \pm \sqrt{\left(\frac{1}{T_m}\right)^2 - 4\frac{K_P K_m}{T_m}}}{2} \tag{176.24}$$

Two values of K_P provide insight. When $K_P = 0$, the closed-loop poles are located at

$$s = \begin{cases} 0 \\ -\dfrac{1}{T_m} \end{cases} \tag{176.25}$$

corresponding to the open-loop pole locations. When K_P is selected such that the radical in Equation 176.24 vanishes,

$$K_p = \frac{1}{4K_m T_m} \tag{176.26}$$

the two roots are located at

$$s = \begin{cases} -\dfrac{1}{2T_m} \\ -\dfrac{1}{2T_m} \end{cases} \tag{176.27}$$

When $0 \le K_p \le 1/(4K_m T_m)$, the closed-loop poles of the system are purely real. When $K_p > 1/(4K_m T_m)$, the closed-loop poles of the system are complex conjugates with a constant real part of $-1/(2T_m)$. Increasing the proportional gain beyond $1/(4K_m T_m)$ only increases the imaginary component of the poles; the real part does not change. A graphical portrayal of the pole locations of the system under proportional control is shown in the root locus plot of Figure 176.6. The poles start at their open-loop positions when $K_P = 0$, and transition to a break point at $-1/(2T_m)$ when $K_p = 1/(4K_m T_m)$. After the break point, they travel parallel to the imaginary axis with only their imaginary parts increasing while their real parts remain constant at $-1/(2T_m)$. It is clear from Figure 176.6 that only specific combinations of ω_{nd} and ζ_d can be achieved with the proportional control configuration. Such relationships can be observed directly via a variety of controls design tools for both single-variable and multivariable systems [Kurfess and Nagurka, 1993, 1994].

Proportional Derivative (PD) Control

To improve performance beyond that available by proportional control, PD control can be employed. The dynamics for the PD controller are given by

$$K(s) = K_D s + K_P \tag{176.28}$$

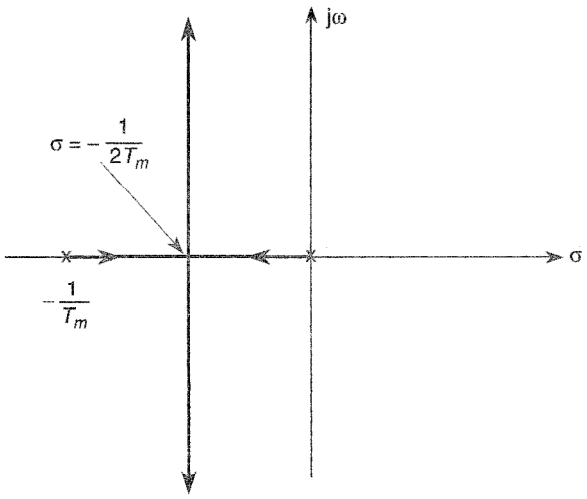

FIGURE 176.6 Root locus for proportional control on a single link.

where the constants K_P and K_D are the proportional and derivative gains, respectively. Employing Black's Law with the PD controller, the closed-loop transfer function for the single actuator-link model is

$$G_{CL}(s) = \frac{\frac{K_m}{T_m}\left(K_D s + K_P\right)}{s^2 + \left(\frac{K_m K_D + 1}{T_m}\right)s + K_m K_P / T_m} \tag{176.29}$$

There are now additional dynamics associated with the zero (root of the transfer function numerator) located at

$$s = -\frac{K_P}{K_D} \tag{176.30}$$

These dynamics can affect the final closed-loop response. Ideally, the zero given in Equation (176.30) will be far enough to the left of the system poles on the s-plane that the dominant pole theory applies. (This would mean the dynamics corresponding to the zero are sufficiently fast in comparison to the closed-loop pole dynamics that their effect is negligible.)

Expressions for K_P and K_D can be found by equating the closed-loop characteristic Equation (176.29),

$$s^2 + \left(\frac{K_m K_D + 1}{T_m}\right)s + K_m K_P / T_m = 0 \tag{176.31}$$

to the target closed-loop characteristic equation that possesses the desired natural frequency and damping ratio, Equation (176.17). Equating the coefficients of s^0 and solving for K_P yields

$$K_P = \omega_{nd}^2 \frac{T_m}{K_m} \tag{176.32}$$

Similarly, equating the coefficients of s^1 and solving for K_D yields

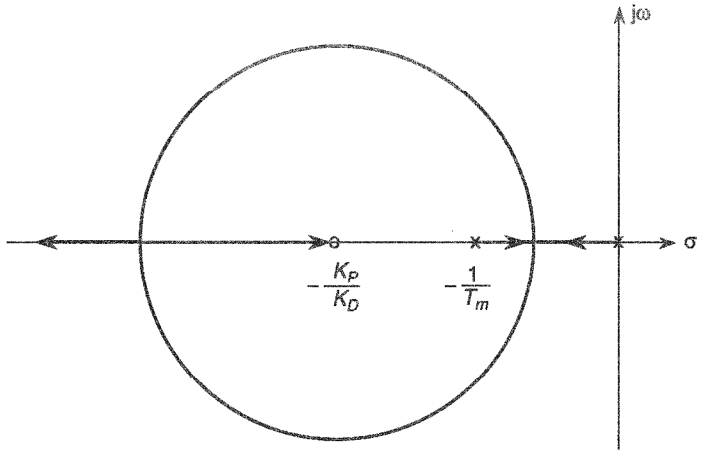

FIGURE 176.7 Root locus for PD control on a single link.

$$K_D = \frac{2\zeta_d \omega_{nd} T_m - 1}{K_m} \tag{176.33}$$

This approach of solving for control gains is known as pole placement. As with all control design methods, the gains derived using Equations (176.32) and (176.33) should be checked to ensure that they are realistic.

Figure 176.7 presents a typical root locus plot for a single actuator-link model using a PD controller where the forward loop gain is varied. The location of the single zero ($s = -K_p/K_D$) can be seen on the real axis in the left of the s-plane. For this design, the zero dynamics will be insignificant in comparison to the pole dynamics. It is noted that the break point for the root locus presented in Figure 176.7 is slightly to the left of the break point in Figure 176.6 ($s = -1/2T_m$). Furthermore, the locus of the complex conjugates poles is circular and centered at the zero.

Classical control tools such as the root locus are critical in control design. Without such tools the designer could use the relationships given by Equations (176.32) and (176.33) to place the poles at any location. However, the resulting location of the zero may have been too close to the closed-loop poles resulting in system dynamics that do not behave as desired. This is described in detail in the following section.

Effect of Zero Dynamics

To demonstrate the effect of a zero, consider two systems that have the same damping ratios (ζ) and natural frequencies (ω_n). The first system is given by

$$G_1(s) = \frac{R_1(s)}{C(s)} = \frac{\omega_n^2}{s^2 + 2\zeta\omega_n s + \omega_n^2} \tag{176.34}$$

and the second system is

$$G_2(s) = \frac{R_2(s)}{C(s)} = \frac{s + \omega_n^2}{s^2 + 2\zeta\omega_n s + \omega_n^2} \tag{176.35}$$

where the input is $c(t)$ and the output is $r_i(t)$ (i = 1,2). The difference between the two systems is the zero located at $s = -\omega_n^2$ for the system described by Equation (176.35). For a unit step input,

$$C(s) = \frac{1}{s} \tag{176.36}$$

the unit step responses of the two systems are

$$R_1(s) = \frac{\omega_n^2}{s^2 + 2\zeta\omega_n s + \omega_n^2}\left(\frac{1}{s}\right) \tag{176.37}$$

and

$$R_2(s) = \frac{s + \omega_n^2}{s^2 + 2\zeta\omega_n s + \omega_n^2}\left(\frac{1}{s}\right) = \frac{s}{s^2 + 2\zeta\omega_n s + \omega_n^2}\left(\frac{1}{s}\right) + \frac{\omega_n^2}{s^2 + 2\zeta\omega_n s + \omega_n^2}\left(\frac{1}{s}\right) \tag{176.38}$$

The difference between the two responses is the derivative term, corresponding to the first term on the right side of Equation (176.38):

$$\frac{s}{s^2 + 2\zeta\omega_n s + \omega_n^2}\left(\frac{1}{s}\right)$$

The time domain responses for Equations (176.37) and (176.38), respectively, are

$$r_1(t) = 1 - e^{-\zeta\omega_n t}\left[\left(\frac{\zeta}{\sqrt{1-\zeta^2}}\right)\sin(\omega_d t) + \cos(\omega_d t)\right] \tag{176.39}$$

and

$$r_2(t) = \left\{1 - e^{-\zeta\omega_n t}\left[\left(\frac{\zeta}{\sqrt{1-\zeta^2}}\right)\sin(\omega_d t) + \cos(\omega_d t)\right]\right\} + \left\{e^{-\zeta\omega_n t}\left(\frac{1}{\omega_n\sqrt{1-\zeta^2}}\right)\sin(\omega_d t)\right\} \tag{176.40}$$

where ω_d, the damped natural frequency, is given by

$$\omega_d = \omega_n\sqrt{1-\zeta^2} \tag{176.41}$$

Several items are worth noting. First, Equations (176.39) and (176.40) are valid for $0 \le \zeta < 1$. Second, the difference between the two responses is

$$\left\{e^{-\zeta\omega_n t}\left(\frac{1}{\omega_n\sqrt{1-\zeta^2}}\right)\sin(\omega_d t)\right\} \tag{176.42}$$

which is the impulse response of the system given by Equation (176.34). For the initial transient of the step response, the impulse response is positive and, therefore, adds to the overall system response. This indicates that the overshoot may be increased, which is the case for the example shown in Figure 176.8 for $\omega_n = 1$ rad/s and $\zeta = 0.707$. In Figure 176.8, the proportional term is the step response given by Equation (176.39), the derivative term is given by expression (176.42), and the total response is given by the sum of the two expressions in Equation (176.40).

From this example, the addition of the zero results in increased overshoot. The real part of the poles is

$$s = \zeta\omega_n = 0.707 \tag{176.43}$$

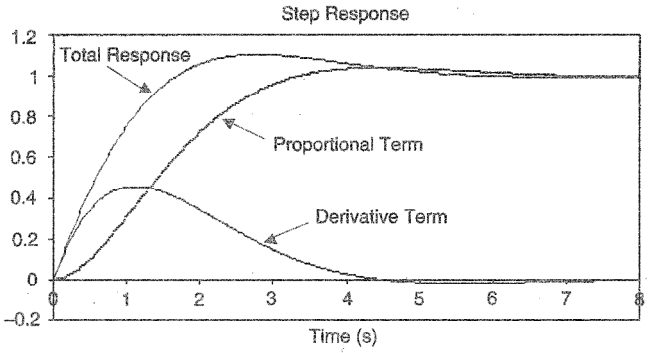

FIGURE 176.8 Step response of two systems.

and the location of the zero is

$$s = 1 \tag{176.44}$$

Thus, the dominant pole theorem does not hold and the dynamics of the zero cannot be ignored. Again, this is demonstrated by the increased overshoot illustrated in Figure 176.8.

Proportional Integral Derivative (PID) Control

A PID controller can be designed to provide better steady-state disturbance rejection capabilities compared to PD or P controllers. The form of the PID controller is given by

$$K(s) = K_D s + K_P + \frac{K_I}{s} = \frac{K_D s^2 + K_P s + K_I}{s} \tag{176.45}$$

For the single actuator-link model, the closed-loop transfer function using a PID controller is given by

$$G_{CL}(s) = \frac{\frac{K_m}{T_m}\left(K_D s^2 + K_P s + K_I\right)}{s^3 + \left(\frac{K_m K_D + 1}{T_m}\right)s^2 + \frac{K_m K_P}{T_m}s + \frac{K_m K_I}{T_m}} \tag{176.46}$$

The closed-loop dynamics are third order and, in comparison to the second-order PD case, the control design has an extra gain that must be determined and an additional pole, located at $s = -d$, added to the target dynamics. The closed-loop characteristic equation,

$$s^3 + \left(\frac{K_m K_D + 1}{T_m}\right)s^2 + \frac{K_m K_P}{T_m}s + \frac{K_m K_I}{T_m} = 0\,, \tag{176.47}$$

is equated to the new target closed-loop characteristic equation,

$$\left(s^2 + 2\zeta_d \omega_{nd} s + \omega_{nd}^2\right)(s + d) = 0 \tag{176.48}$$

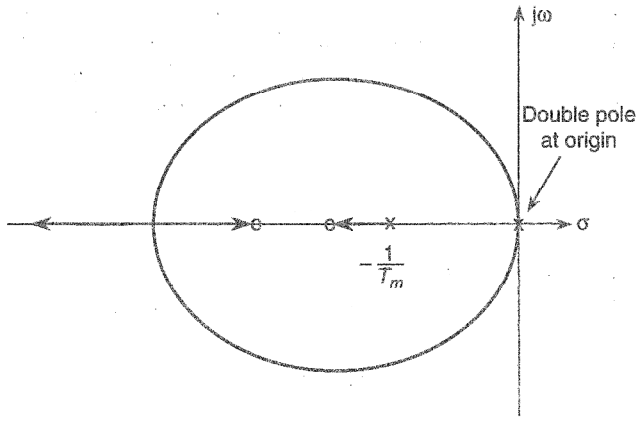

FIGURE 176.9 Root locus for PID control on a single link.

As with the PD controller, the location of the zeros in Equation (176.46) as well as the extra pole at $s = -d$, should have a negative real parts that are at least three times as negative as the target closed-loop pole locations.

Figure 176.9 presents a possible root locus plot for the single actuator-link model with a PID controller where the forward loop gain is varied. The two zeros and extra pole can be seen on the real axis to the left in the s-plane. As with the PD control design, the gains used for achieving the target dynamics must be well understood. It is easy to pick gains that move both zeros and the extra pole far to the left in the s-plane. However, it should be noted that the further left the dynamics are shifted in the s-plane, the faster they become, influencing less the overall response of the system. However, to increase the response speed of these dynamics requires higher gains that ultimately result in higher power requirements (and the possibility of instability). As such, while designing for higher gains is rather straightforward mathematically, the implementation may be limited by the physical constraints of the system.

Unlike the locus of the complex conjugate poles for the model employing PD control (Figure 176.6), the locus here need not be circular. Also, given the increased number of closed-loop system parameters (including the control gains and design parameters such as d, the sensitivity of the closed-loop dynamics to changes of these parameters may be important and should be investigated. For example, if the proportional gain changes a small amount (which is bound to happen in a real system), the impact in the overall system performance must be understood. Mathematically, sensitivity can formally be shown to be a complex quantity (having both magnitude and angle), and a variety of techniques can be used to explore sensitivity to parameter changes [Kurfess and Nagurka, 1994].

176.5 Method of Computed Torque

If the robot is a direct-drive type without gear reduction or if the command inputs are not slowly varying, the control scheme of the previous section may exhibit poor performance characteristics and instability may even result. One method of compensating for the effects of link coupling is to use feed-forward disturbance cancellation. The disturbance torque is computed from the robot dynamic equation, summarized in vector-matrix form as

$$\tau = D(\theta)\ddot{\theta} + C(\theta,\dot{\theta}) + G(\theta) + F(\dot{\theta}) \tag{176.49}$$

where τ is the $n \times 1$ vector of joint torques (forces), $D(\theta)$ is the $n \times n$ inertia matrix, $C(\theta,\dot{\theta})$ is the $n \times 1$ vector of Coriolis and centrifugal torques (forces), $G(\theta)$ is the $n \times 1$ vector of torques (forces) due to gravity, and $F(\theta)$ is the $n \times 1$ vector of torques (forces) due to friction. In the feed-forward disturbance

cancellation scheme, the right side of Equation (176.49) is computed using the desired value of the joint variables and injected as a compensating "disturbance." If the plant is minimum phase (has no right-half *s*-plane zeros), its inverse is also fed forward to achieve tracking of any reference trajectory.

Another version of computed-torque control, known as *inverse dynamics control*, involves setting the control torque to

$$\tau = D(\theta)v + C(\theta,\dot{\theta}) + G(\theta) + F(\dot{\theta}) \tag{176.50}$$

which results in $\ddot{\theta} = v$, a double integrator system. The value of v is now chosen as $v = \ddot{\theta}_d + K_D(\dot{\theta}_d - \dot{\theta}) + K_P(\theta_d - \theta)$ where subscript d denotes desired. This results in the tracking error, $e = \theta_d - \theta$, which satisfies

$$\ddot{e} + K_D\dot{e} + K_P e = 0 \tag{176.51}$$

The gains K_P and K_D can be chosen for the desired error dynamics (damping and natural frequency). In general, computed-torque control schemes are computationally intensive due to the complicated nature of Equation (176.49), and require accurate knowledge of the robot model [Bonitz, 1995].

176.6 Cartesian Space Control

The basic concept of Cartesian space control is that the error signals used in the control algorithm are computed in Cartesian space, obviating the solution of the inverse kinematics. The position and orientation of the robot end-effector can be described by a 3×1 position vector, p, and the three orthogonal axes of an imaginary frame attached to the end effector. (The axes are known as the normal (n), sliding (s), and approach (a) vectors.) The control torque is computed from

$$\tau = D(\theta)\ddot{\theta} + C(\theta,\dot{\theta}) + G(\theta) + F(\dot{\theta}) \tag{176.52}$$

$$\ddot{\theta} = J(\theta)^{-1}[\ddot{x}_d + K_D\dot{e} + K_P e - \dot{J}(\theta,\dot{\theta})\dot{\theta}] \tag{176.53}$$

where $J(\theta)$ is the manipulator *Jacobian* that maps the joint velocity vector to the Cartesian velocity vector, $\ddot{x}_d$ is the 6×1 desired acceleration vector, $e = [e_p^T e_o^T]^T$, e_p is the 3×1 position error vector, e_o is the 3×1 orientation error vector, K_D is the 6×6 positive-definite matrix of velocity gains, and K_P is the 6×6 positive-definite matrix of position gains. The actual position and orientation of the end-effector is computed from the joint positions via the forward kinematics. The position error is computed from $e_p = \theta_d - \theta$ and, for small error, the orientation error is computed from $e_o = \frac{1}{2}[n \times n_d + s \times s_d + a \times a_d]$. The control law of Equations (176.52) and (176.53) results in the Cartesian error equation,

$$\ddot{e} + K_D\dot{e} + K_P e = 0 \tag{176.54}$$

The gain matrices K_D and K_P can be chosen to be diagonal to achieve the desired error dynamics along each Cartesian direction [Spong and Vidyasagar, 1989].

The Cartesian space controller has the disadvantage that the inverse of the Jacobian is required, which does not exist at *singular configurations*. The planned trajectory must avoid singularities, or alternative methods such as the SR pseudoinverse [Nakamura, 1991] must be used to compute the Jacobian inverse [Bonitz, 1995].

Defining Terms

Cartesian or task space — The set of vectors describing the position and orientation of the end-effector using coordinates along orthogonal axes. The position is specified by a 3×1 vector of the

coordinates of the end-effector frame origin. The orientation is specified by the 3×1 normal, sliding, and approach vectors describing the directions of the orthogonal axes of the frame. Alternately, the orientation may be described by Euler angles, roll/pitch/yaw angles, or an axis/angle representation.

Forward kinematics — The function that maps the position of the joints to the Cartesian position and orientation of the end-effector. It maps the joint space of the manipulator to Cartesian space.

Inverse kinematics — The function that maps the Cartesian position and orientation of the end-effector to the joint positions. It is generally a one-to-many mapping, and a closed-form solution may not always be possible.

Jacobian — The function that maps the joint velocity vector to the Cartesian translational and angular velocity vector of the end-effector $\dot{x} = J(\theta)\dot{\theta}$.

Singular configuration — A configuration of the manipulator in which the manipulator Jacobian loses full rank. It represents configurations from which certain directions of motion are not possible or when two or more joint axes line up and there is an infinity of solutions to the inverse kinematics problem.

References

Black, H. S., Stabilized feedback amplifiers, *Bell Syst. Tech. J.*, January 1934a.

Black, H. S., Stabilized Feedback Amplifiers, U.S. Patent No. 2,102,671, 1934b.

Bonitz, R. G., Robots and controls. In *The Engineering Handbook*, Dorf, R. D., Ed., CRC Press, Boca Raton, FL, 1995.

Hogan, N., Impedance control: an approach to manipulation, parts I, II, and III. *ASME J. Dynamic Syst. Meas. Control*, 107, 124, 1985.

Kurfess, T. R. and Nagurka, M. L., A geometric representation of root sensitivity, *ASME J. Dynamic Syst. Meas. Control*, 116, 305–309, 1994.

Kurfess, T. R. and Nagurka, M. L., Foundations of classical control theory with reference to eigenvalue geometry, *J. Franklin Inst.*, 330, 213–227, 1993.

Kurfess, T. R. and Jenkins, H. E., Ultra-high precision control, in *Control Systems Applications*, Levine, W., Ed., , CRC Press, Boca Raton, FL, 2000, p. 212.

Kurfess, T. R., Precision manufacturing, in *Mechanical System Design Handbook*, Nwokah, O. and Hurmuzlu, Y., Eds., CRC Press, Boca Raton, FL, 2002, p. 151.

Luh, J. Y. S., Conventional controller design for industrial robots — a tutorial, *IEEE Trans. Syst. Man. Cybern.*, SMC-13, 298–316, 1983.

Luh, J. Y. S., Walker, M. W., and Paul, R. P., Resolved-acceleration control of mechanical manipulators, *IEEE Trans. Automat. Control*, AC-25, 464, 1980.

Nagurka, M. L. and Kurfess, T. R., An alternate geometric perspective on MIMO systems, *ASME J. Dynamic Syst. Meas. Control*, 115, 538, 1993.

Nagurka, M. L. and Kurfess, T. R., A Unified Classical/Modern Approach for Undergraduate Control Education, lecture notes from National Science Foundation Workshop, 1992.

Nakamura, Y., *Advanced Robotics, Redundancy, and Optimization*, Addison-Wesley, Reading, MA, 1991.

Raibert, M. H. and Craig, J. J., Hybrid position/force control of manipulators, *ASME J. Dynamic Syst. Meas. Control*, 103, 126, 1981.

Spong, M. W. and Vidyasagar, M. *Robot Dynamics and Control*, John Wiley & Sons, New York, 1989.